4-2001

GPS-determination of along-strike variation in Cascadia margin kinematics: Implications for relative plate motion, Subduction zone coupling, and permanent deformation

M. Meghan Miller

Daniel J. Johnson

Charles M. Rubin

Herb Dragert

Kelin Wang

See next page for additional authors

Authors

M. Meghan Miller, Daniel J. Johnson, Charles M. Rubin, Herb Dragert, Kelin Wang, Anthony Qamar, and Chris Goldfinger

TECTONICS, VOL. 20, NO. 2, PAGES 161-176 APRIL 2001

GPS-determination of along-strike variation in Cascadia margin kinematics: Implications for relative plate motion, subduction zone coupling, and permanent deformation

M. Meghan Miller[1], Daniel J. Johnson[1], Charles M. Rubin[1], Herb Dragert[2], Kelin Wang[2], Anthony Qamar[3], and Chris Goldfinger[4]

Abstract. High-precision GPS geodesy in the Pacific Northwest provides the first synoptic view of the along-strike variation in Cascadia margin kinematics. These results constrain interfering deformation fields in a region where typical earthquake recurrence intervals are one or more orders of magnitude longer than the decades-long history of seismic monitoring and where geologic studies are sparse. Interseismic strain accumulation contributes greatly to GPS station velocities along the coast. After correction for a simple elastic dislocation model, important residual motions remain, especially south of the international border. The magnitude of northward forearc motion increases southward from western Washington (3-7 mm/yr) to northern and central Oregon (~9 mm/yr), consistent with oblique convergence and geologic constraints on permanent deformation. The margin-parallel strain gradient, concentrated in western Washington across the populated Puget Lowlands, compares in magnitude to shortening across the Los Angeles Basin. Thus crustal faulting also contributes to seismic hazard. Farther south in southern Oregon, northwestward velocities reflect the influence of Pacific-North America motion and impingement of the Sierra Nevada block on the Pacific Northwest. In contrast to previous notions, some deformation related to the Eastern California shear zone crosses northernmost California in the vicinity of the Klamath Mountains and feeds out to the Gorda plate margin.

1. Introduction

The Cascadia convergent margin, located between two migrating triple junctions, deforms in response to superimposed forces of North America, Juan de Fuca, and Pacific boundary interactions (Figure 1), including oblique subduction and entrainment of the Sierra Nevada and Oregon Coast Range blocks. Infrequent great earthquakes along the Cascadia subduction zone together with frequent, smaller earthquakes within the North America and downgoing Juan de Fuca plates characterize seismic risk in the Pacific Northwest. The kinematics and dynamics of the Cascadia subduction zone have proved particularly elusive to seismologic studies, owing to relatively low Benioff-Wadati zone seismicity and short historical earthquake records [*Heaton and Kanamori*, 1984].

During the last decade, however, new tools in paleoseismology have revealed a rich Holocene seismic record including evidence for recurring catastrophic coastal subsidence, tsunamis, and ground shaking [*Atwater*, 1987; *Adams*, 1990; *Atwater et al.*, 1995; *Darienzo and Peterson*, 1995; *Satake et al.*, 1996; *Atwater and Hemphill-Haley*, 1997]. Taken together with evidence for a circum-Pacific tsunami [*Satake et al.*, 1996] and local tree ring histories [*Atwater and Yamaguchi*, 1991; *Yamaguchi et al.*, 1997], these data point to a major earthquake on the Cascadia subduction zone late in January, 1700 A.D. On the basis of the size of the tsunami in Japan, the entire length of the Cascadia margin likely broke in a single event of *Mw*~9.0 at that time [*Satake et al.*, 1996]. Whether this size of rupture also typifies earlier events has been considered. The simultaneity of turbidite triggering in tributary and trunk submarine canyons and channels along the length of the Cascadia margin during the Holocene supports the case for large (*Mw*~9) earthquakes that rupture the length of the convergent margin rather than smaller events along a seismically segmented subduction zone [*Adams*, 1990; *Nelson et al.*, 2000]. The turbidite data further suggest recurrence for such events on average every ~600 years. Nevertheless, sparse empirical constraints on the interplay between Juan de Fuca-North America convergence and crustal faulting within the North America plate have prevented characterization of the processes that drive deformation.

High-precision geodesy samples the deformation field over timescales of years or decades. Separation of mutually interfering deformation fields from plate boundary and crustal faults hinges on our ability to accurately model or measure processes that independently contribute to the integrated, instantaneous velocity field. These processes include (1) convergence between the Juan de Fuca and North American plates (Figure 2 and Table 1) [*Riddihough*, 1984; *Wilson*, 1993; *DeMets and Dixon*, 1999; this study], (2) elastic and viscoelastic strain that accumulates in the forearc of the subduction zone in response to seismogenic coupling between the young and buoy-

[1]Department of Geological Sciences, Central Washington University, Ellensburg, Washington
[2]Geological Survey of Canada, Pacific Geoscience Center, Sidney, British Columbia, Canada
[3]Geophysics Program, University of Washington, Seattle, Washington.
[4]College of Oceanic and Atmospheric Sciences, Oregon State University, Corvallis, Oregon.

Paper number 2000TC001224.
0278-7407/01/2000TC001224$12.00

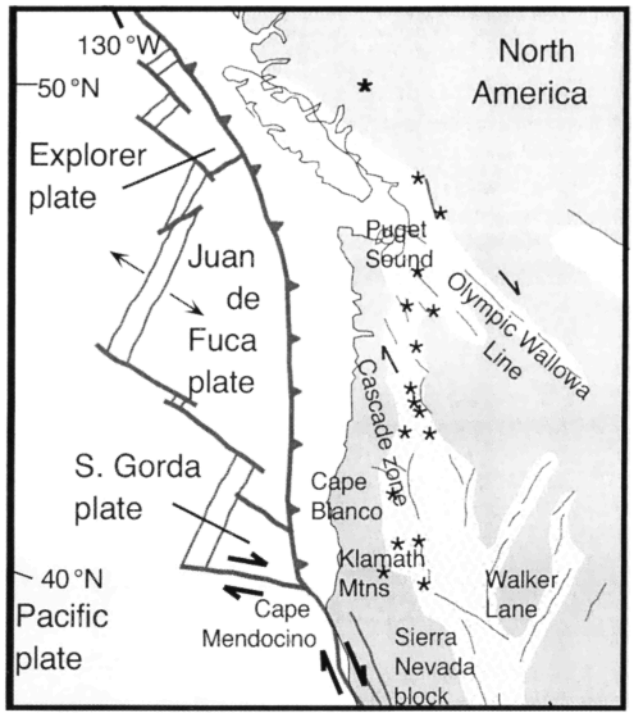

Figure 1. Tectonic setting of the Cascadia margin. The Juan de Fuca plate convergent margin lies between two migrating triple junctions. Because of entrainment of the western margin of North America in Pacific plate motion, the Pacific Northwest deforms in response to the interaction of all three plates. Stippled areas show actively deforming zones, and asterisks show volcanic vents associated with the continental arc. Modified from *Pezzopane and Weldon* [1993].

ant Juan de Fuca plate and the Cascadia forearc [*Dragert et al.*, 1994; *Heaton and Kanamori*, 1984], (3) partitioned deformation within North America due to oblique convergence, (4) distribution of primarily northwest directed dextral shear related to Pacific-North America plate motion that ultimately penetrates the continent in southern California and feeds into the Cascadia arc and back arc region [*Pezzopane and Weldon*, 1993] and into the forearc (this study), and (5) impingement of the Basin and Range on the back arc of southeastern Washington and its northward transition to back arc contraction. Resolution of contributions from these processes require observations of regional deformation in an internally consistent, robust, and stable realization of the North America reference frame as well as a model that corrects for the first-order effects of interseismic strain accumulation. Continuous Global Positioning System (GPS) results from the Pacific Northwest Geodetic Array (PANGA) provide the first synoptic view of Pacific Northwest deformation along the Cascadia margin and place first-order constraints on processes that contribute to continental deformation.

These geodetic results bear on convergent margins around the world. Careful differentiation of the interseismic strain that results from subduction zone coupling and secular deformation on crustal faults illuminates the processes that drive deformation within plate margins and constrains seismic risk. These results confirm that GPS geodesy provides a critical tool for rapidly characterizing Earth deformation processes and constraining seismic potential.

2. Methods and Results

PANGA, a network of continuously operating GPS receivers distributed throughout the Pacific Northwest in the United States and Canada, is deployed and supported by an international consortium of institutions and agencies [*Miller et al.*, 1998]. Within the Western Canada Deformation Array [*Dragert and Hyndman*, 1995], the oldest component of PANGA, deformation constraints are well characterized. PANGA monitors crustal deformation with millimeter-level precision by deter-

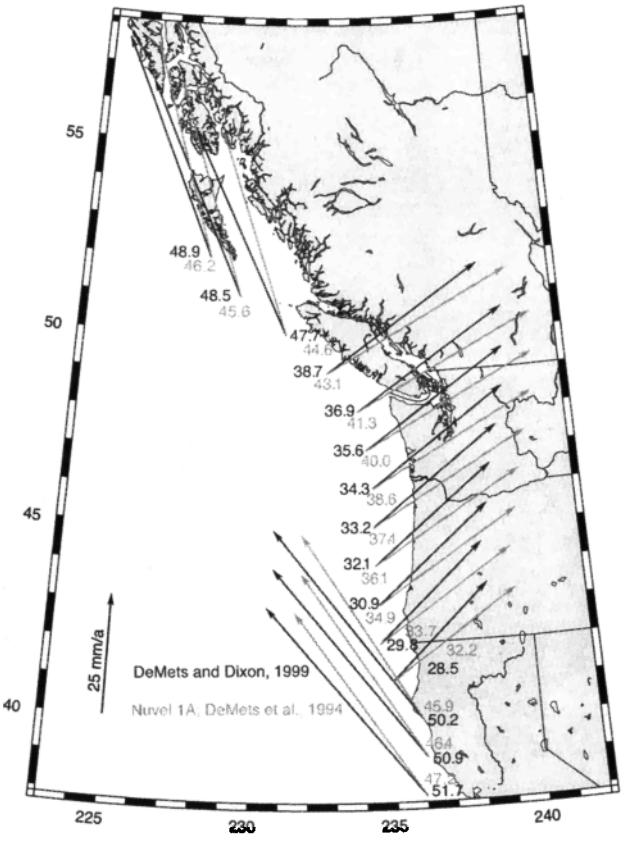

Figure 2. Comparison of relative plate motion velocities along the Cascadia margin. Light shaded arrows plot the azimuth and magnitude of Pacific and Juan de Fuca plate motion relative to North America, as predicted by NUVEL-1A [*DeMets et al.*, 1994], solid arrows from Table 1. The motion of the Juan de Fuca plate is constrained by magnetic lineations that record its motion relative to the Pacific plate. Thus changes in the Pacific–North America relative motion pole affect predicted Juan de Fuca-North America convergence. The new euler pole for Juan de Fuca–North America plate motion (Table 1) lies closer to the Juan de Fuca plate, and thus more rotation is implied, and the rate increases from south to north. A more northerly relative plate motion azimuth results in nearly orthogonal convergence along the Canadian Cascadia margin.

Table 1. Relative Plate Motion Euler Poles, North America, Pacific and Juan de Fuca Plates

Plate pair	Cartesian coordinates		
	Ωx μrad/yr	Ωy μrad/yr	Ωz μrad/yr
PCFC-NAnew[a]	0 002328	-0 007983	0.010440
PCFC-NA N1A[b]	0 001768	-0.008439	0.009817
PCFC-JUAN[c]	0 006710	0 003770	0 004150
JdF - 1-PCFC[d]	0 006510	0 003170	0.005080
NAnew-JUAN(2)[e]	0.004382	0.011753	-0 006290
NAnew-JUAN(1)[f]	0 004182	0 011153	-0 005360

[a]Recent Pacific–North America pole reported by *DeMets and Dixon* [1999]. Globally distributed GPS results led them to reassess the NUVEL-1A pole for comparison Consequent refinement of the data quality criteria for the global plate circuit resulted in revision of the Pacific–North America euler pole.

[b]This is the NUVEL-1A Pacific North America pole for reference [*DeMets et al.*, 1994].

[c]This pole, originally reported by *Wilson* [1993], describes the motion of the Juan de Fuca plate relative to the Pacific plate since magnetic anomaly 2A. It is incorporated into NUVEL-1A by *DeMets et al.* [1994]

[d]Wilson's alternate Pacific–Juan de Fuca pole (JdF1 of *Wilson* [1993]).

[e]Our preferred North America–Juan de Fuca pole. We propagate *DeMets and Dixon's* [1999] Pacific–North America pole and *Wilson's* [1993] preferred Pacific–Juan de Fuca pole to the North America–Juan de Fuca pole.

[f]The *DeMets and Dixon* [1999] Pacific–North America pole and *Wilson*'s [1993] Pacific–Juan de Fuca pole (1), propagated to a North America–Juan de Fuca pole.

mining daily positions for each station within the network and measuring its motion through time, with respect to motion of other stations on stable North America (Figures 2 and 3).

2.1. GPS Observations and Uncertainties

GPS phase data were analyzed using GPS Inferred Positioning System/Orbit Analysis and Simulation Software (GIPSY/OASIS II), developed by the Jet Propulsion Laboratory (JPL) for NASA, using the precise point-positioning technique and JPL-generated fiducial-free orbit solutions [*Zumberge et al.*, 1997]. Daily solutions for individual station position and corresponding matrices of the covariance among the three position components were determined within the International Terrestrial Reference Frame (ITRF 97) [*Boucher et al.*, 1999] without ambiguity resolution. For this study, daily and seasonal irregularities in the global reference frame were minimized using a regional stabilization based on subtracting average common-mode position variations at six sites (ALBH, CABL, DRAO, GOBS, PABH, and QUIN, Plate 1). This technique [*Bock et al.*, 1997; *Wdowinski et al.*, 1997] is particularly useful in cases where the length of observations is short, and hence the relative effect of uncorrected seasonal noise is potentially large. Using GIPSY/OASIS II, daily positions accumulated over a 2–6 year period yield station velocities by least squares fit to the individual station time series, which take into account covariance among the three position components (Table 2).

Both white noise and time-correlated noise characterize GPS velocity estimates. Time-correlated noise effects include potential monument motion unrelated to crustal deformation [*Langbein and Johnson*, 1997], uncertainty in the satellite orbit parameters, and atmospheric and local environmental effects [*Mao et al.*, 1999]. Pure white noise models underestimate uncertainty [*Johnson and Agnew*, 1995]; however, time-correlated noise estimates, to date, largely rely on a priori assumptions about monument behaviors that are not well determined for a wide variety of geodetic monuments in realistic settings. PANGA uses a variety of regionally available GPS stations that include different styles of monumentation in a variety of geologic settings; in addition, different atmospheric effects are likely across the network that spans 10° in latitude as well as a longitudinal maritime zone and mountain range.

We adopted a simple empirical model for estimating the GPS rate error σ_r for the three velocity components, north, east, and vertical (Table 2) for coordinate time series in the presence of combined white and time-correlated noise [*Mao et al.*, 1999]:

$$\sigma_r^2 \cong \frac{12\sigma_w^2}{gT^3} + \frac{a\sigma_f^2}{g^b T^2} + \frac{\sigma_{rw}^2}{T} \qquad (1)$$

where g is the number of measurements per year, T is the total time span of observations, a and b are empirical constants (a=1.78 and b=0.22), σ_w and σ_f are the white and "flicker" noise magnitudes (in mm), and σ_{rw} is random walk noise (in mm/$\sqrt{\text{yr}}$). White and flicker noise depend on sampling frequency and duration, while random walk noise only depends on observation interval. Nevertheless, high-frequency time series are required to characterize the processes that contribute to the error budget. Weighted root mean squared from time series of position for individual stations was used to scale these contributing processes [*Dixon et al.*, 2000; *Miller et al.*, 2001]. Monument noise has been characterized as a random walk process [*Langbein and Johnson*, 1997], which becomes a detectable contributor to the error budget after ~4 years [*Mao et al.*, 1999]. A priori estimates of random walk are included in this error model according to monument type.

2.2. North America Reference Frame

ITRF provides a global reference frame with station positions and velocities based on the International GPS Service (IGS) network. It relies on a global minimization of the velocities for all IGS stations included in a particular version of ITRF. Two common approaches are used to constrain the transformation from a particular version of ITRF to a North American plate frame. One relies on a published transformation euler pole; the other includes sufficient stations from the stable continent to solve for an euler pole for the internally consistent data set. We used the latter approach.

Both approaches can have pitfalls. For instance, time-correlated noise from individual station velocity determina-

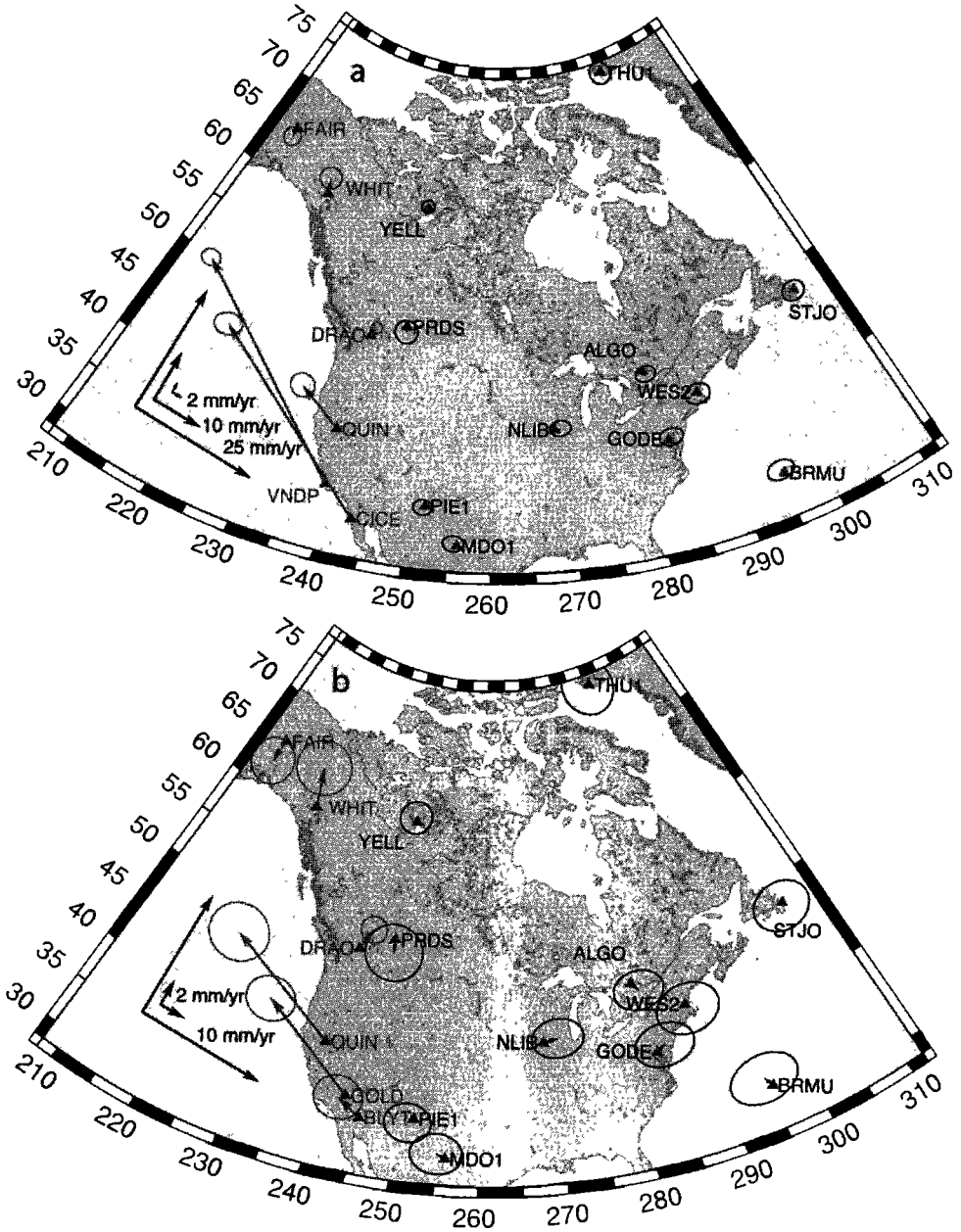

Figure 3. Realization of GPS-determined North America reference frame. Eleven GPS stations from the continental interior and Atlantic passive margin shown as solid vectors (ALGO, BRMU, GODE, MDO1, NLIB, PIE1, PRDS, STJO, THU1, WES2, and YELL) define the North American reference frame (Table 3). Each plot shows the same data set at different vector scales, with reference velocities indicated by shaded vectors plotted at the same scale. (a) The smaller vector scale emphasizes goodness of fit for the ITRF 97–North America euler vector; the scale allows Pacific plate station reference velocities to be shown. Only one reference frame station residual exceeds 1 mm/yr (BRMU). (b) The larger vector scale emphasizes that the small residuals are not systematic within regions potentially affected by isostacy, and reference velocities come from the deforming North America plate margin (Pacific plate velocities are too large to plot at this scale). Error ellipses on both plots represent two-dimensional 95% confidence regions, using the error model of *Mao et al.* [1999], discussed in text, and their propagation in the reference frame inversion.

tions may yield detectably different velocities for different time spans. In our case, the velocity of Penticton, which has relatively strong annual signals even after regional stabilization, differs on the order of tenths of a mm/yr. The quality and geometry of coverage of the stable plate interior potentially contribute another source of error, but temporal and spatial sampling are good in North America. Different versions of ITRF may have systematic differences in velocities or euler poles determined for a particular version or time interval may not be directly comparable to others. For instance, we observe

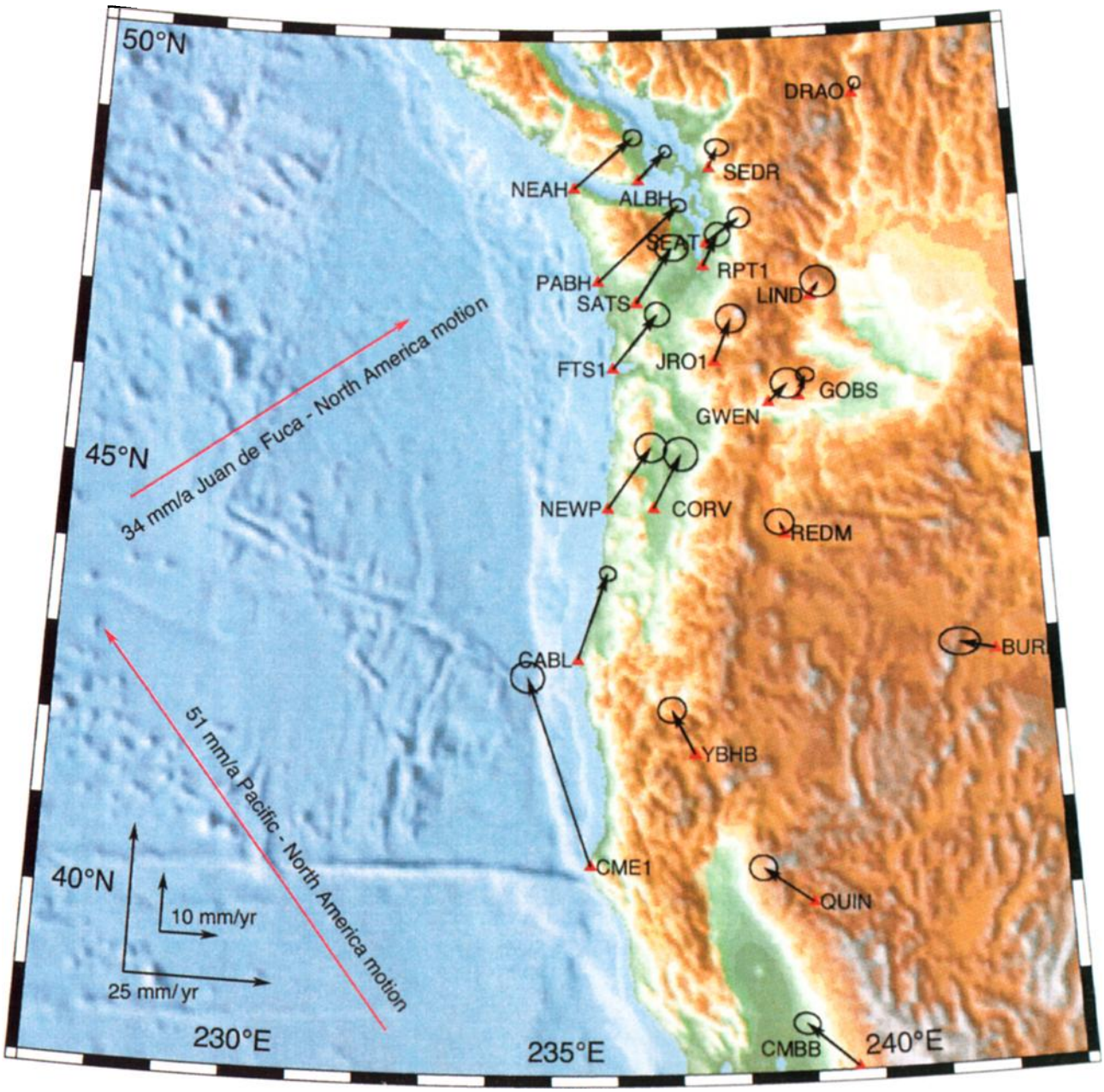

Plate 1. GPS-determined velocity field, Pacific Northwest Geodetic Array (PANGA). This velocity field is plotted relative to North America, as defined by 11 GPS stations in the continental interior and Atlantic passive margin (Table 3 and Figure 3). Two to six years of data from continuously operating GPS stations yield PANGA station velocities. Error ellipses show two-dimensional 95% confidence regions. Seafloor topography from *Smith* and *Sandwell* [1997].

Table 2. Regional GPS Station Velocities in the International Terrestrial Reference Frame (ITRF 97)

Station	Longitude, °E	Latitude, °N	E Velocity, mm/yr	N Velocity mm/yr	E Velocity Sigma	N Velocity Sigma	Correlation
ALBH	236.51	48.39	-7 75	-11.42	0.33	0 30	-0.01543
ALGO	281.93	45.96	-16 38	-0 51	0 73	0 55	0.02290
BRMU	295.30	32.37	-12.79	6 13	1.02	0.67	-0.00233
BURN	242.16	42.78	-18.36	-12 98	1.38	0 89	-0.06392
CABL	235.44	42 84	-6.08	-1.95	0.50	0 40	-0 02650
CMBB	239.61	38.03	-19 40	-7.69	0.87	0.68	-0.08200
CME1	235.60	40 44	-21.12	15.33	1.13	1 01	-0.02596
CORV	236.70	44.59	-7.89	-7.93	1.14	1.11	-0 04273
DRAO	240.38	49.32	-12.70	-13.51	0.33	0.31	-0.00882
FAIR	212.50	64.98	-7.70	-23.08	0.61	0.61	-0.01726
FTS1	236.04	46.20	-4 36	-7.23	0 83	0.76	-0.04602
GOBS	239 19	45.84	-11.25	-11.93	0.56	0.40	-0 03226
GODE	283.17	39.02	-14.18	0.97	0.88	0.61	0.01040
GWEN	238 67	45.78	-9 13	-12 45	1.08	0.97	-0.03578
JRO1	237 78	46.28	-9 43	-8 70	1.00	0 92	-0 01393
LIND	239.46	47.00	-11.30	-13.11	1.17	1.03	-0.06032
MDO1	255.99	30.68	-11.71	-9.63	0.74	0 57	0.00272
NEAH	235 38	48.30	-2.32	-7.95	0.56	0 47	0.01405
NEWP	235.94	44.59	-4.32	-6.14	1.06	0.95	-0.01390
NLIB	268.43	41.77	-14.18	-4.96	0.75	0.55	0.06023
PABH	235.80	47.21	1.60	-3.57	0.46	0.35	-0 03359
PIE1	251.88	34.30	-12.06	-11 66	0.66	0.54	0.01438
PRDS	245.71	50.87	-14.73	-14.38	0.85	0.82	-0.03486
QUIN	239.06	39.97	-19.55	-9.35	0.89	0 83	-0.02753
REDM	238 85	44 26	-12.88	-13.58	0.97	0.82	-0 02492
RPT1	237 63	47.39	-9.90	-10.68	0 82	0 74	-0 00965
SATS	236.46	46.97	-6.10	-6.98	1.13	0 85	-0.02427
SEAT	237.69	47.65	-6.92	-11 80	0.70	0.63	-0.00979
SEDR	237.78	48.52	-11.32	-12.50	0.76	0.50	-0 06398
STJO	307 32	47.60	-15 75	9.69	0 85	0 67	-0.02896
THU1	291.21	76.54	-22.21	3.71	0.70	0.83	-0.00857
WES2	288.51	42.61	-15.69	2.37	0.93	0.72	0.03063
WHD1	237.30	48.31	-8.14	-11.69	0.89	0.81	-0.01917
YBHB	237.29	41.73	-15.07	-8.46	0.94	0.82	0.06363
YELL	245.52	62.48	-16.81	-13.2	0.42	0.43	-0.02150

a systematic north bias for western North America between ITRF 96 and ITRF 97. Finally, the application of regional stabilization may also introduce systematic biases to velocities in the ITRF frame, making use of published euler poles less robust than determinations that rely on a uniform analysis.

We determine GPS station velocities with reference to GPS-defined North America (Figure 3, Plate 1, and Table 3). Velocities for PANGA together with a collection of global stations were determined within ITRF 97 [*Boucher et al.*, 1999]. We use 11 stations east of the North American Cordillera to establish an internally consistent North America reference frame (Figure 3). The realization of North America specifically excludes Penticton (DRAO), British Columbia, and Fairbanks (FAIR), Alaska, as well as other stations that lie west of the Cordilleran deformation front, which we suspect of lying within the deforming plate boundary. The uncertainty estimates for the ITRF 97 velocities (Table 2) are formally propagated in the solution for the ITRF 97–North America euler pole (Figure 3, Plate 1 and Table 3). Thus 95% confidence intervals show the combined uncertainty estimates of the GPS observations and reference frame propagation (Figure 3 and Plate 1). For the stations used to define North America (Table 3), no residual velocity estimates exceed 1.1 mm/yr, and only one exceeds 1 mm/yr (BRMU, Figure 3 and Table 3). Penticton moves relative to North America 1.7±0.4 mm/yr directed northeast, a velocity larger than the largest residual motion from any stations that define the reference frame (Table 3). At the 95% confidence level the North America realization and resulting network velocities are very consistent with our previous solutions that relied on ITRF 96 using a similar approach with somewhat sparser coverage. Our strategy allows us to solve di-

Table 3. PANGA and Select GPS Station Velocities, Relative to GPS-Defined North America

GPS Station	Longitude, °E	Latitude, °N	E Velocity, mm/yr	N Velocity, mm/yr	E Velocity Sigma	N Velocity Sigma	Correlation
			Stations Defining North America[a]				
ALGO	281 93	45 96	0 46	-0 62	0 77	0.59	0.03160
BRMU	295 30	32.37	-0.40	0.69	1.07	0.71	0.03970
GODE	283.17	39.02	0.66	0.38	0.92	0 64	0 02850
MDO1	255.99	30.68	-0.66	0.30	0.80	0.61	-0 02970
NLIB	268 43	41.77	1.08	0.22	0 79	0 58	0.05610
PIE1	251 88	34 30	-0 41	-0 35	0 72	0 58	-0 02870
PRDS	245 71	50.87	0 05	-0 98	0 88	0.85	-0 03370
STJO	307.32	47.60	-0 17	-0 22	0 88	0 73	0 00330
THU1	291 21	76 54	-0.12	-0.11	0 76	0.86	-0 05380
WES2	288.51	42 61	0.12	-0 34	0 96	0 75	0.04420
YELL	245 52	62 48	-0.13	0 28	0 48	0 49	0 05050
			Regional PANGA Stations				
ALBH	236.51	48.39	4.67	4.81	0 40	0 41	-0 07750
BURN	242 16	42.78	-5 97	1.54	1 40	0.93	-0.07270
CABL	235.44	42.84	5.11	14.51	0.56	0 49	-0.10220
CMBB	239.61	38 03	-8.46	7.61	0.91	0 73	-0.11240
CME1	235 60	40.44	-10 34	31.76	1 16	1.05	-0.04660
CORV	236.70	44.59	4 80	9 06	1 17	1.14	-0.06170
DRAO	240.38	49.32	0.73	1 58	0 40	0.41	-0 04540
FAIR	212.50	64.98	-0.06	-1 72	0 64	0 71	-0.01730
FTS1	236.04	46.20	7.57	9.14	0.86	0.81	-0.06410
GOBS	239 19	45 84	1 33	3 54	0 61	0 48	-0 07060
GWEN	238.67	45.78	3.32	3.09	1.11	1.01	-0.04620
JRO1	237.78	46.28	2 94	7 15	1.03	0.96	-0.02710
LIND	239.46	47.00	1.51	2.26	1 19	1 06	-0.06610
NEAH	235.38	48.30	9.91	8 52	0 60	0.55	-0.02620
NEWP	235.94	44.59	7.35	10 27	1 09	0.99	-0.03050
PABH	235.80	47.21	13.70	12.81	0.52	0 45	-0.08420
QUIN	239 06	39 97	-8 32	6 08	0 93	0.87	-0.05440
REDM	238 85	44 26	-0.75	1.94	1.00	0.86	-0 04210
RPT1	237.63	47.39	2 62	5.19	0 85	0.79	-0 02660
SATS	236 46	46.97	6.10	9.22	1.15	0.89	-0 03600
SEAT	237 69	47.65	5.68	4 07	0 74	0.69	-0 03130
SEDR	237 78	48.52	1 46	3 35	0 79	0.57	-0.07560
YBHB	237.29	41.73	-3.76	7 49	0 97	0.86	0.03130

[a]The euler pole from ITRF 97 to this 11-station GPS-defined North America plate is located at 1 49±1.85°N, 101 62±0 66°E, with an angular rotation of 0.2058±0 0036 °/Myr

rectly for differences in various versions of ITRF, resulting in a robust realization of the North America reference frame.

2.3. Model Correction for Interseismic Strain Accumulation

The two largest contributors to GPS-observed deformation in the Pacific Northwest, forearc migration and Cascadia interseismic strain accumulation, result in two highly oblique mutually interfering deformation fields. Their obliquity allows their separation through simultaneous inversion. Forearc-Juan de Fuca convergence and seismogenic coupling control the pattern and magnitude of interseismic deformation. Independent constraints on plate convergence, taken with geometric singularities of the deformation field, constrain a dislocation model. The dislocation model presented here, referenced to North America, establishes the motion of the forearc with respect to the continent. In contrast, most previously published models are referenced to the station Penticton (DRAO, Plate 1).

In other respects we adopt the approach of *Fluck et al.* [1997]. The model fault (Figure 4) approximates the subduction zone fault by smooth profiles for the depth of the structure determined from various geophysical techniques, including depth contours defined by Benioff-Wadati seismicity, seismic reflection, seismic refraction, teleseismic waveform analysis, and seismic tomography [*Fluck et al.*, 1997]. The complexity of the natural fault plane makes a model fault com-

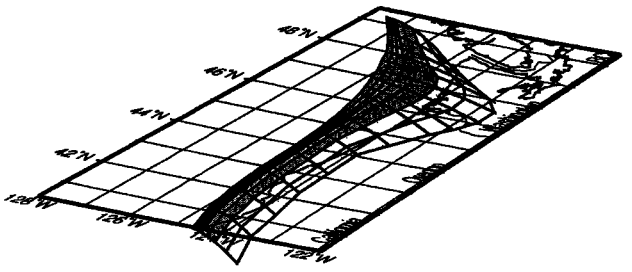

Figure 4. Perspective view of the locked portion of the Cascadia subduction zone model thrust fault. View from the southeast extends from northern California in the lower right to southern British Columbia in the upper right. Dark shading indicates full locking, light shading indicates the transition zone where locking decreases down-dip from 100% to full slip in a linear fashion. At depths below the model fault, the subduction zone fault moves at the full plate convergence rate. After *Fluck et al.* [1997].

posed of triangular elements desirable rather than rectangular fault segments. This accounts for the known curvature of the plate boundary and the inferred arch in the downgoing slab (Figure 4). Adjustments for the depth of the model fault approximate the actual depth of the fault below topography (which increases from the submarine deformation front to the Cascade crest) rather than below an arbitrary horizontal datum. The relatively smooth locked and transition zones rely on a compilation of heat flow data, vertical deformation results, and independent horizontal deformation constraints and may not be realistic in detail, based on the complexity of the vertical deformation field [*Pezzopane and Weldon*, 1993]. Because of an emphasis on thermal constraints, the width of the locked and transition zones correlates to the shallowness of the slab [*Fluck et al.*, 1997]. Slip is then applied to the planar triangular elements that compose this model fault. Contributions to surface deformation from all elements are numerically integrated. The calculation is optimized for the accuracy of the solution (relative to a three-dimensional analytical solution on a rectangular fault) and for computing time [*Fluck et al.*, 1997]. Full interplate slip is applied to the locked zone, and a linear down-dip decrease characterizes the transition zone. The dislocation is applied as back slip [*Savage*, 1983], in contrast to deep slip models that also model long-term fault block motions.

Thus our approach accepts the fault geometry, locking area of the megathrust, and integrated back slip dislocation approach of *Fluck et al.* [1997], but we reassess the convergence

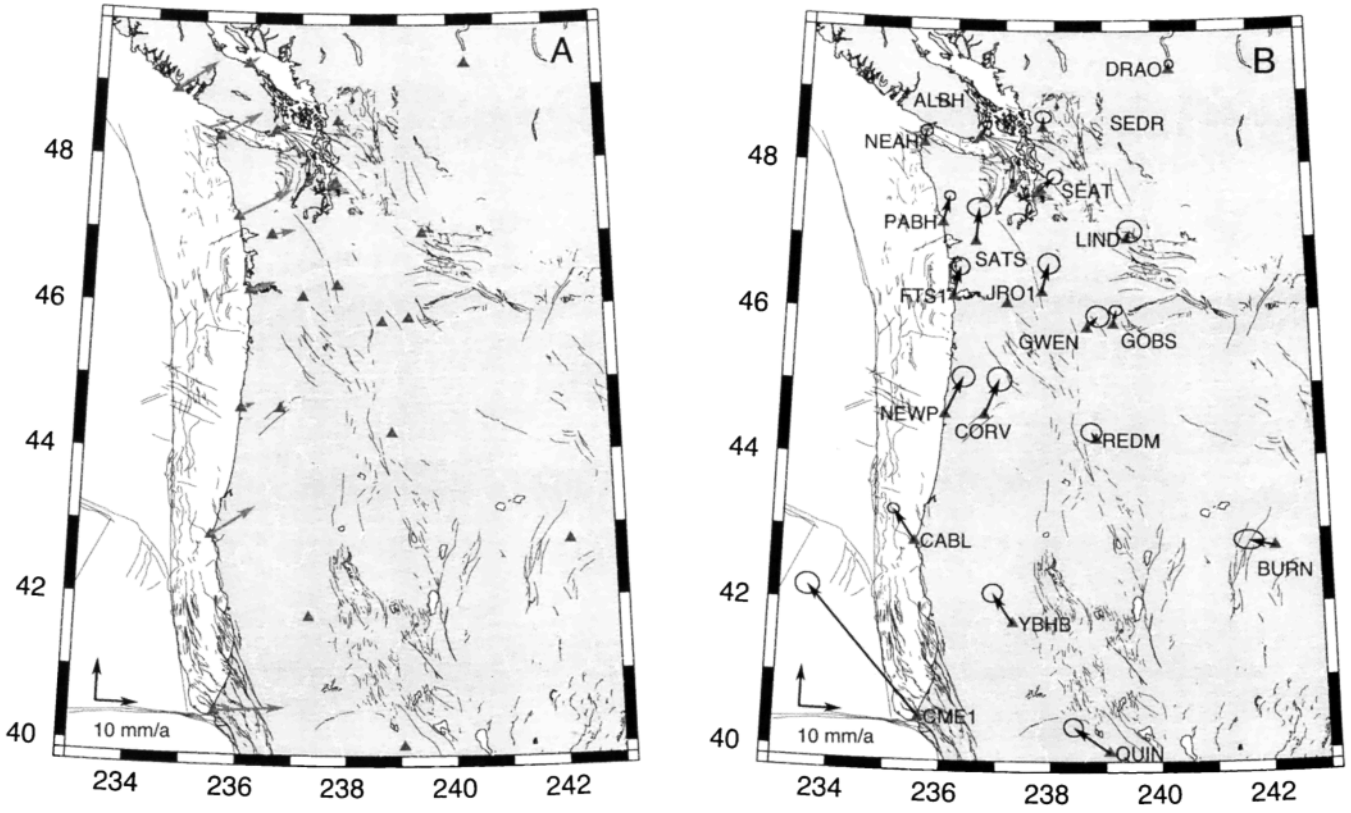

Figure 5. PANGA station velocities with model velocities from elastic dislocation modeling and residual station velocities. All velocities are relative to North America (see Figure 3). (a) Predictions of the forearc–Juan de Fuca dislocation model at PANGA stations. Slip azimuth and magnitude varies along strike and the model. (b) Residual velocities. GPS-determined velocities are corrected for annualized elastic deformation that results from coupling along the Cascadia subduction zone, using predicted motions in Figure 5a (see Table 4). The residual velocities partly reflect geologic deformation; other effects are detailed in text. Faults were compiled from *Gower et al.* [1985] and *Slemmons et al.* [1992].

rate and direction, and solve for convergence between the forearc and the Juan de Fuca plate in an interative fashion. The model of *Fluck et al.* [1997] assumes a uniform convergence velocity and direction along the strike length of the Cascadia margin. We develop an along-strike slip-variant model that incorporates a new constraint on global plate motions [e.g., *DeMets and Dixon*, 1999].

Along convergent margins such as Cascadia, direct estimates of relative plate motion are precluded because evidence is subducted rather than preserved. Thus convergence direction and magnitude derive from a circuit that goes from the North America plate through the Pacific plate to the Juan de Fuca plate, where magnetic anomalies allow estimates of relative motion [e.g., *Riddihough*, 1984; *Wilson*, 1993]. Using established estimates of the Pacific–Juan de Fuca euler vectors [*Wilson*, 1993], we propagate the recently revised North America–Pacific euler vector determined by *DeMets and Dixon* [1999] to a new euler vector for Juan de Fuca–North America convergence (Table 1). This results in an euler pole that lies closer to the Juan de Fuca plate, which in turn, results in a larger rotation of Juan de Fuca relative to North America than that implied by NUVEL-1A (Figure 2). In order to best evaluate the impact of the along-strike variation in convergence direction and magnitude we divide the plate boundary into 11 contiguous model fault segments along strike and vary the slip magnitude and azimuth on each patch, consistent with the new euler pole. We then integrate the contribution of each of the megathrust segments to elastic dislocation at each geodetic station from model calculations. This estimate of recoverable deformation is then subtracted from the GPS velocity determinations to yield a residual velocity field.

Because the actual motion of the forearc determines the local convergence rate and direction, iterative model runs use the residual velocities to determine forearc-Juan de Fuca convergence. Stations near the coast are quite sensitive to changes in the model convergence direction (Figure 5a). Stations farther east in the forearc are more sensitive to the shape of the slab than the convergence direction and provide a more robust estimate of forearc motion. When the residual velocities of coastal stations agree with those farther inland yet still in the fore-arc, the model is stable.

The residual velocities (observed GPS velocity less the estimate of recoverable deformation, Figure 5) provide a first order estimate for permanent deformation along crustal structures, but also includes any mismodeling of the subduction zone, local effects of elastic strain accumulation along other faults, deformation effects related to complexity in the deforming southern Gorda plate, or spurious contributions to measurements. We compare these residual velocities to predictions of integrated geologic rates constrained by neotectonic, paleomagnetic, and seismic moment determinations [*Pezzopane and Weldon*, 1993; *Wells et al.*, 1998]. Ultimately, the subduction zone model will be refined to reflect new constraints that are emerging from more localized studies [e.g., *Khazaradze et al.*, 1999; *Murray and Lisowski*, 2000; *McCaffrey et al.*, 2000; *Savage et al.*, 2000], to reflect differing velocities of crustal blocks within the forearc with respect to North America, and to account for viscoelastic effects [*Wang et al.*, 2000] Our study evaluates the robustness of the current subduction zone model and the pattern of residual velocities in comparison with independent determinations.

3. Discussion

3.1. Instantaneous Velocity Field

Continuous GPS results in the Pacific Northwest provide a remarkably coherent view of along-strike variation in Cascadia margin deformation (Plate 1), characterized by four important tectonic domains. (1) Coastal stations in the northern and central parts of the margin are strongly entrained in the Juan de Fuca–North America convergence direction, although the northward component of station velocities increases from north to south. (2) The California-southern Oregon boundary reflects a composite velocity that includes the San Andreas transform system, Mendocino triple junction migration, and interaction between North America and the south Gorda plate. The Klamath Mountains are partially entrained with the impinging Sierra Nevada block, and Eastern California shear zone deformation previously believed to penetrate the arc and back arc is at least partly distributed back out to the plate boundary. (3) Inland stations have lesser motions, consistent with their structural domains from south to north: the Canada and northern Washington back arc experiences slow convergence parallel motion, the Yakima fold belt actively contracts, and southeastern Oregon shows integrated Basin and Range extension.

Our velocity field differs somewhat from recent Pacific Northwest GPS results; one important aspect is the realization of the North American reference frame. Some studies report results relative to Penticton, British Columbia (DRAO) [*Dragert et al.*, 1994; *Dragert and Hyndman*, 1995; *Khazaradze et al.*, 1999], which is a well established and long-observed station in the Western Canada Deformation Array and the IGS. These results do not directly compare to those in a North America reference frame, although baseline comparisons are possible. Some other recent studies are reported in a North America reference frame. For the Cape Blanco transect [*Savage et al.*, 2000], North America is defined by simultaneous analysis of a subset of stations that define the stable plate, in a similar fashion as ours. A key difference with our analysis is that slightly fewer (seven) stations define North America and both Penticton and Fairbanks (DRAO and FAIR, Figure 3) are included. These two stations have detectable motion relative to North America in our stabilization (Figure 3) and introduce a northward bias to the Cape Blanco velocity field. *McCaffrey et al.* [2000] take a different approach, using a published euler pole to convert from ITRF 96 to the North American reference frame. This approach can be vulnerable to time-dependent error sources and differences in analysis strategy that may propagate into the reference frame as discussed above. The results presented here have been tested for stabilization of 9-11 North American stations over two generations of ITRF and several versions of the

PANGA velocity solution. While the euler pole changes among solutions, the residual field of stations used in the plate definition is robust and is stable well within the 95% confidence interval.

3.2. Signature of Convergence Direction and Magnitude

Juan de Fuca plate magnetic anomalies [*Riddihough*, 1984; *Wilson*, 1993] and global plate circuits [*DeMets et al.*, 1994] yield several million year averages of plate convergence history, although recent revision in the Pacific-North America euler pole [*DeMets and Dixon*, 1999] implies important changes to Juan de Fuca-North America convergence (Figure 2 and Table 1). Propagating the revised Pacific–North America euler pole [*DeMets and Dixon*, 1999] through the Juan de Fuca plate [*Wilson*, 1993] yields a new set of Juan de Fuca–North America convergence rates and directions (Table 1 and Figure 2). The new pole yields orthogonal convergence along the northern Cascadia margin, in Canada, consistent with the convergence direction inferred from GPS results along that part of the margin [*Henton et al.*, 1998]. This convergence-parallel component of velocity decays markedly with distance from the coast, consistent with the predictions of elastic dislocation due to coupling along the subduction zone (Figure 4). To the south of the international boundary, more highly oblique predicted convergence occurs along the northerly striking margin. As a consequence, the model attributes a greater proportion of the north component of GPS velocities to interseismic elastic strain accumulation (Figure 5). The northward component is partially restored by adding forearc motion into the model, but the along-strike rotation persists. Recent dislocation models based on spatially denser but geographically restricted networks indicate misfit to a pure subduction model [e.g., *Khazaradze et al.*, 1999; *McCaffrey et al.*, 2000; *Savage et al.*, 2000]. The strong effects of forearc migration accompany subduction zone coupling along the coast from Washington to southern Oregon (Plate 1). In southern Oregon and northern California, the south Gorda plate actively deforms and the elastic model is consequently weak.

3.3. Geologic Deformation Within the North America Plate

Active deformation zones transect the Pacific Northwest separating stable crustal blocks and feeding dextral shear from the continental interior back out to the plate margin (Figure 1) [*Pezzopane and Weldon*, 1993], which has resulted in rotation of blocks within the forearc [*England and Wells*, 1991]. Tectonically active regions of faulting within the forearc, arc, and back arc separate more stable crustal blocks and partition deformation. Most crustal faults accommodate directed north-south deformation or, in the south, dextral northwest-directed slip that reflects a relationship to Pacific-North America motion (Figure 1). For instance, the Eastern California shear zone and Walker Lane ultimately feed slip into seismically and tectonically active regions in the Pacific Northwest (Figures 1 and 6).

3.3.1. Pattern and magnitude of forearc deformation. When corrected for the coupling effects of the megathrust, described above, the velocity field can also be used to evaluate long term or permanent deformation rates (Figure 5). To first order the residual velocity field approximates the permanent deformation field yet also may include possible elastic effects of smaller crustal faults as well as any misfit of the subduction zone model.

North of the international border the GPS observations are largely explained by subduction zone coupling. Nominal residual velocities, systematically directed to the northeast, span the region as far east as Penticton (DRAO, Figure 5) and cannot be attributed to purely elastic coupling as they lack a gradient related to distance from the fault. The northward component of velocity abruptly increases across northwestern Washington, implying a marked strain gradient within the Washington forearc. The monotonic increase to 7 mm/yr in southern Washington implies commensurate crustal shortening. The pattern indicates north-south directed contraction within the forearc. Young marine strata off the coast of Washington show evidence of north-south directed folding and faulting [*McCrory*, 1996]. Young, east-west striking reverse faults within densely populated regions of Puget Sound, such as the Seattle fault, Whidbey Island fault, and the Toe Jam fault, accommodate an important part of this contraction budget [*Johnson et al.*, 1996]. The Seattle fault was likely responsible for an earthquake with fault displacement of 7 m some 900-1100 years ago [*Bucknam et al.*, 1992]. Focal mechanisms [*Crosson*, 1972; *Weaver and Smith*, 1983; *Ma et al.*, 1991; *Wang et al.*, 1995; *Ma et al.*, 1996] and geologic evidence [*Johnson et al.*, 1994; *Pratt et al.*, 1997; *Johnson et al.*, 1999] suggest that such shallow seismicity in the Puget basin reflects north-south directed contraction. Between 1939 and 1965, four earthquakes greater than magnitude 6 occurred in the southern Puget Sound area, although the most damaging were within the down going Juan de Fuca plate [*Ludwin et al.*, 1991].

This strain gradient marks the northern margin of the migrating forearc that characterizes latitudes from central Oregon to central Washington. This northward migration was previously known from geologic evidence [e.g., *Wells et al.*, 1998] and has recently been described by spatially denser GPS observations concentrated in coastal Oregon [*McCaffrey et al.*, 2000]. Our data indicate northward forearc migration of 9 mm/yr at central Oregon latitudes.

The Cascade deformation zone (Figure 1) comprises stepping Holocene normal and dextral faults along the extensional southern Cascade arc in Oregon, in the region of the magmatic front, that extend from Mount Lassen to Mount Rainier (Figures 1 and 6). This zone delineates a step in the northward component of velocity [*McCaffrey et al.*, 2000, Figure 2]. The two 1993 Klamath Falls earthquakes, magnitudes 5.9 and 6.0, occurred within this zone of distributed shear [*Braunmiller et*

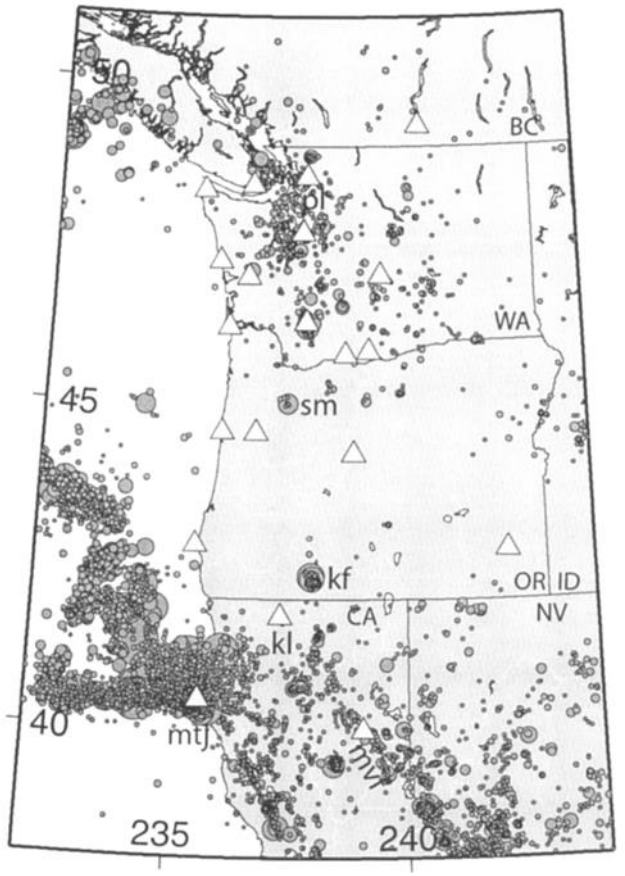

Figure 6. Regional seismicity in the Pacific Northwest. Seismic events with $M \geq 3$ from the Council of the National Seismic System catalog (1969 to 2000) are scaled by magnitude. Locations include: pl, Puget Lowlands; sm, Scott's Mills; kf, Klamath Falls; kl, Klamath Mountains; mtj, Mendocino triple junction; mvf, Mohawk Valley fault zone. Triangles show the locations of GPS stations (see Plate 1 and Figure 5 for velocities). Denser distributions of earthquakes occur in the areas where strain gradients are implied by GPS velocities, both in northern California and within the Puget Lowlands of western Washington. Diffuse seismicity also characterizes the back arc in central Washington.

al., 1995; *Dreger et al.*, 1995; *Nabelek and Xia*, 1995], as did the 1993 M 5.5 Scotts-Mills earthquake near Portland [*Nabelek and Xia*, 1995]. Crustal seismicity is concentrated along the Mount St. Helens seismic zone [*Malone et al.*, 1981; *Weaver et al.*, 1981; *Qamar et al.*, 1987] and continues northward to Mount Rainier [*Crosson*, 1972]. Seismicity in western Washington has not been correlated in detail with mapped surface faults, in part because of heavy vegetation, thick Quaternary glacial deposits, and alluvium.

It is noteworthy that before the dislocation model correction is applied, there is apparent convergence across the Cascade zone that forms the prominent, arc-axial escarpment in Oregon (see BURN and CABL vectors, Plate 1). With the subduction zone model correction, extension across the Cascade graben is implied (Figure 5b), consistent with several mm/yr of west directed dilation. In southern Oregon, the Cascade zone is well positioned to account for the apparent "double locked zone" from the inversion of *McCaffrey et al.* [2000], which we interpret as a known active normal fault superimposed on the eastward decaying recoverable deformation field from the subduction zone. This structure coincides with the eastern limit of forearc migration in Oregon.

Farther to the south at Cape Blanco (CABL, Figure 5b), the northward velocity of the migrating forearc falls off only slightly, by 1 mm/yr, raising the possibility of modest north directed extension in southern Oregon. While the residual velocity at Cape Blanco is highly model dependent, it agrees well with the Yreka velocity (see CABL and YBHB, Table 4 and Figure 5b) that is insensitive to the model corrections. Northwestward velocities at Cape Blanco and Yreka point to the southward increasing influence of Pacific plate interactions along the Gorda segment of the Cascadia boundary. These dominate even farther south at Cape Mendocino.

Several factors contribute to the very large residual motion at Cape Mendocino (33.5 ±1.0 mm/yr directed 341°); its velocity suggests that it lies more on the Pacific plate than North America. The Eastern California shear zone and faults of the San Andreas system such as the Ma'acama and Bartlett Springs faults lie farther east. In particular, 22.1 +6.2/-4.7 mm/yr of the velocity at Cape Mendocino may be attributed to the Ma'acama and Bartlett Springs faults [*Freymueller et al.*, 1999] that lie within the San Andreas system to the east of Cape Mendocino (CME1, Figure 5b) and that feed intra-plate deformation between the triple junction and the Oregon border [*Kelsey and Carver*, 1988; *McCrory*, 2000]. Another 11.0±0.8 mm/yr, directed 311° lies to the east of Quincy (QUIN, Figure 3 and Table 2), presumably on a northward extension of the Eastern California shear zone [*Miller et al.*, 2001] and Walker Lane [*Oldow et al.*, 2001]. This leaves a negligible amount that must be accounted for. Together with elastic strain accumulation related to the San Andreas fault and Mendocino transform, these faults contribute to the large northwestward station velocity. Model edge effects also may concentrate near Cape Mendocino, which lies near three major plate boundary structures. Nevertheless, the residual velocity at Cape Blanco is concordant with Pacific plate motion.

Taking into account the faults of the San Andreas system, the northern California–southern Oregon data imply a velocity gradient between Cape Blanco and the stations at Quincy, Yreka, and Cape Mendocino (CABL, QUIN, YBHB, and CME1, Figure 5 and Table 4). While the residual velocities at Cape Blanco and Cape Mendocino are sensitive to model assumptions, negligible model velocities at Yreka and Quincy make them independent of the elastic model and its possible errors. The Sierra Nevada block moves ~ 14 mm/yr northwestward with respect to North America; Quincy (QUIN, Plate 1 and Figure 5) is separated from the Sierra Nevada block to the west by the Mohawk Valley fault zone [*Dixon et al.*, 2000]. Some 2-3 mm/yr of the 14 mm/yr that make up the Eastern California shear zone penetrate west of Quincy (Figure 5) as evidenced by

Table 4. Residual Velocities From the Dislocation Model

GPS Station	Longitude, °E	Latitude, °N	E Velocity, mm/yr	N Velocity, mm/yr	E Velocity Sigma	N Velocity Sigma	Correlation
ALBH	236 51	48.39	1.43	2 95	0.40	0.41	-0.07750
BURN	242.16	42.78	-6.17	1 52	1 40	0.93	-0.07270
CABL	235 44	42.84	-5 12	7.52	0.56	0.49	-0.10220
CMBB	239.61	38.03	-8.51	7.62	0 91	0.73	-0.11240
CME1	235.60	40.44	-26.87	30 72	1 16	1.05	-0.04660
CORV	236.70	44 59	3.44	8.63	1.17	1 14	-0.06170
DRAO	240.38	49.32	0.29	1.36	0.40	0 41	-0.04540
FTS1	236.04	46 20	1.51	7.16	0.86	0 81	-0.06410
GOBS	239.19	45 84	0.72	3.44	0.61	0.48	-0.07060
GWEN	238.67	45.78	2.60	2.98	1.11	1.01	-0.04620
JRO1	237 78	46.28	1.68	6 97	1.03	0.96	-0.02710
LIND	239.46	47.00	0.83	2.10	1 19	1.06	-0 06610
NEAH	235.38	48 30	0.40	2.81	0.60	0 55	-0.02620
NEWP	235.94	44 59	4.16	9 05	1 09	0.99	-0 03050
PABH	235.80	47.21	1.45	6.35	0 52	0.45	-0 08420
QUIN	239.06	39.97	-8.54	6.11	0.93	0.87	-0.05440
REDM	238 85	44.26	-1.26	1 83	1.00	0.86	-0 04210
SATS	236.46	46.97	0.61	8.04	1.15	0 89	-0.03600
SEAT	237.69	47.65	3.93	3 55	0 74	0 69	-0.03130
SEDR	237 78	48.52	0.13	2.72	0 79	0.57	-0 07560
YBHB	237 29	41.73	-4.88	7.25	0 97	0.86	0 03130

diffuse seismicity in the region (Figure 6). Another gradient of 4 mm/yr lies between Yreka and Cape Blanco (YBHB and CABL, Figure 5) in the vicinity of the Klamath Mountains (Figures 1 and 6). Thus nearly half of the strain budget related to the Eastern California shear zone and entrainment of the Sierra Nevada block is diminished across the northern Sierra Nevada and Klamath Mountains.

Faults in southeastern Oregon are also candidates for continuation of the Eastern California shear zone and Walker Lane (Figure 1) [*Wallace*, 1984; *Doser*, 1988; *dePolo et al.*, 1991]. Eastern Oregon faulting occurs in two northwesterly zones that transect the state [*Pezzopane and Weldon*, 1993]. Right-lateral oblique faults displace Pleistocene and Holocene age strata. The Eastern Oregon zones include seismicity and active faulting that is distributed across western Idaho, northeastern Oregon, and southern Washington.

Both impingement of the Sierra Nevada block and oblique subduction have been invoked as processes that drive Oregon forearc migration [*Wang* 1996; *Wells et al.*, 1998]. The kinematics, taken with the geometry of the subduction zone, invite speculation. Vancouver Island, which is part of Wrangellia, arguably forms a more rigid backstop against which the inland penetration of a Pacific transform component terminates. In this view, the Oregon and Washington forearc migrates in front of the impinging Sierra Nevada block. The northern margin of the migrating forearc also coincides with the limit of oblique subduction, however, implying a different origin. The bight in the continent margin results in nearly orthogonal convergence along Vancouver Island, where forearc migration is absent, and moderately oblique convergence farther south, where forearc migration is relatively rapid (Figure 2). This implies that oblique subduction drives forearc migration.

The nature of intraplate deformation that accommodates Cascadia forearc migration has been described as a block rotation. Kinematically consistent fault block models have been developed for larger regions of the deforming margin [*Pezzopane and Weldon*, 1993]. Various independent estimates of the euler vector for forearc–North America motion have been published, based on geologic [*Wells et al.*, 1998] and geodetic data [*McCaffrey et al.*, 2000]. Geodetic estimates may be vulnerable to neglecting elastic and permanent deformation along crustal faults, discrepancies between plate circuit constraints and actual convergence of the fore-arc (resulting in mismodeling of the elastic field), and possible flaws or inconsistencies in reference frame realization. Thus such euler vectors may have little tectonic significance. Nonetheless, the forearc is geologically and geodetically coherent in central and northern Oregon where it is clearly migrating northward. The eastern boundary of the forearc is regionally discrete and corresponds to known seismicity along the magmatic front [*Stanley et al.*, 1996]. Strain gradients that define the northern and southern limit of forearc migration are more complex and characterized by distributed deformation rather than rigid block behavior.

England and Wells [1991] have described the "quasicontinuous" nature of geologic structures that surround the deforming forearc. The strain gradient across the Washington forearc, for instance, is consistent with distributed continental deformation [*Stanley et al.*, 1996], as is the possible boundary between central Oregon migration and southern Oregon–northern California northwestward translation (Figure 5b). Direct geodetic evidence for significant rotation is not evident in the rigid part of the forearc. Furthermore, the geological structures that delineate the edges of the migrating forearc are poorly defined on the basis of current geodetic results.

3.3.2. Structural domains of the deforming back arc. A north-to-south transition in tectonic regimes also characterizes the back arc, although our data are sparse and, within the United States, are partly based on 2 year time series (at LIND, REDM, and BURN, Plate 1). A small but persistent northeast directed velocity of 1.7±0.4 mm/yr at Penticton (DRAO, Figure 5, Plate 1, and Tables 3 and 4) is well established from its long observation history and its inclusion in the ITRF. A similar velocity determination from the central Washington back arc (LIND, Figure 5, Plate 1, and Tables 3 and 4) implies little net deformation occurs between the two stations.

Shortening of ~1 mm/yr between Lind and Goldendale (LIND, GOBS, Figure 5, Plate 1, and Tables 3 and 4) is small but consistent with modest geologic estimates of active contraction across the Yakima fold belt and diffuse seismicity in this region (Figure 6). The Olympic-Wallowa line, a prominent alignment of topographic features, extends from the northern edge of the Olympic Peninsula to northeastern Oregon (Figure 1) [*Raisz*, 1945; *Hooper and Conrey*, 1989; *Mann and Meyer*, 1993]. The northwest-trending lineament comprises northeast facing escarpments at either end and, in central and southern Washington, it forms a major geomorphic and structural boundary in the Neogene Yakima fold belt, illuminated by active faulting and seismicity (Figure 6). The southern extent of the Olympic-Wallowa line records dextral and normal-oblique displacements of Quaternary strata [*Hooper and Conrey*, 1989; *Mann and Meyer*, 1993] and coincident microseismicity [*Zollweg and Jacobson*, 1986]. The right-lateral Milton-Freewater and Arlington-Shuttler Butte fault zones also displace Quaternary strata and probably generated the 1936 Milton-Freewater M ~6.4 earthquake [*Noson et al.*, 1988].

The Olympic-Wallowa line in central Washington has received much attention because of its proximity to the nuclear facilities and waste disposal sites of the Hanford Nuclear Reservation and large hydroelectric dams along the Columbia River [*Tolan and Reidel*, 1989; *Mann and Meyer*, 1993; *Hutter*, 1994]. Our results indicate small but resolvable strain. The Olympic-Wallowa line consists of a series of east-west trending anticlinal ridges and associated thrust faults that mark a kinematic boundary within the Yakima fold belt [*Reidel*, 1984; *Tolan and Reidel*, 1989; *Beeson and Tolan*, 1990]. Shortening occurs across thrust faults and folds within the belt [*Campbell and Bentley*, 1981; *Reidel*, 1984; *Campbell*, 1994; *West et al.*, 1996] that locally cut Quaternary-Holocene (?) strata. Despite common thrust fault focal mechanism solutions in eastern Washington, earthquakes have not been correlated to specific faults. N-S directed maximum stress, inferred from P axes of reverse fault earthquake mechanisms, is consistent with the E-W trending anticlines in the Yakima fold belt [*Malone et al.*, 1975].

The largest historic earthquake in the Pacific Northwest, the 1872 North Cascades or Wenatchee earthquake [*Milne*, 1956] has an estimated M >7 [*Malone and Bor*, 1979]. The exact location, depth and magnitude of the earthquake are poorly determined [*Malone and Bor*, 1979].

To the south of Goldendale (GOBS, Plate 1 and Figure 5b), the northward velocity component decreases and possible (but negligible) extension may be implied between the Columbia River and central Oregon. The northwestward direction of this velocity determination (REDM, Figure 5b) belies the influence of the Basin and Range deformation field. To the southeast, this effect becomes dominant at Burns Junction (BURN, Plate 1 and Figure 5a) which is moving nearly westward 7 mm/yr with respect to the interior of North America. Northwest striking normal faults bound the Goose Lake and other grabens and have low Holocene slip rates [*Bacon et al.*, 1999; *Colman et al.*, 2000]. The 1968 Adel, Oregon, M 5.1 earthquake swarm [*Patton*, 1985] occurred in this zone. The velocity at Burns Junction (BURN, Plate 1 and Figure 5a) reflects the integrated Basin and Range extension that lies to the east.

3.4. Summary

Taken collectively, the residual velocity field yields new insights on the basic pattern of permanent deformation within the Pacific Northwest. The GPS results establish constraints on modern deformation, which support the pattern of deformation suggested by studies that integrate geological and paleomagnetic data [*Wells*, 1990; *Wells et al.*, 1998] and that synthesize neotectonic evidence and seismic moment estimates [*Pezzopane and Weldon*, 1993].

Forearc deformation varies markedly from north to south. Along the Canadian segment, which converges nearly orthogonal to strike of the deformation front, evidence of forearc migration parallel to the subduction zone is absent. Along the central Cascadia margin the signature of northward transport of the forearc predominates, and increases from north to south, consistent with geological evidence for north-south directed shortening in coastal Washington. This results in a strong strain gradient and implied seismic hazard across the Puget lowlands, the most densely populated area of Washington. A major crustal feature crosses the width of the plate margin: the Olympic-Wallowa line extends from the Idaho border to the northwest into Puget Sound and, in the west, is kinematically related to the limit of forearc migration. In Oregon, extension characterizes the high Cascades and coincides with a boundary between the migrating forearc and the modestly deforming back arc.

Along the southern Cascadia margin, northwestward transport reflects the influence of Pacific plate motion [*Kelsey and Carver*, 1988], tectonic complexity of the triple junction region [*Wilson*, 1989; *Kelsey et al.*, 1996; *Freymueller et al.*, 1999], and known crustal faults that partition plate motion. Deformation in northern California is consistent with the slip budget on the San Andreas, Ma'acama, and Bartlett Springs faults. Furthermore, we present new evidence that deformation from the Walker Lane and Eastern California shear zone transects the region of the triple junction and southern Cascadia forearc.

Geomorphic variation in the arc historically raised the possibility of seismic segmentation of the subduction zone.

Our GPS results demonstrate that along-strike variation in convergent margin geomorphology corresponds to patterns of permanent deformation. Taken in the context of paleoseismic, tsunami, tree-ring, and turbidite studies, this geomorphic and kinematic segmentation does not imply seismic segmentation of the subduction zone. Increasing evidence suggests that the megathrust is not seismically segmented, with the possible exception of the south Gorda plate.

4. Conclusions

We present a synoptic view of modern Cascadia margin deformation from GPS observations. Coupling of the subduction zone dominates instantaneous crustal deformation along the extent of the Pacific Northwest coast. This result substantiates the potential for great subduction earthquakes in the Pacific Northwest.

Model corrections for subduction zone locking allow evaluation of deformation on crustal faults, which also contribute significantly to regional seismic risk. Station density is relatively sparse, yet existing models for subduction zone geometry and locking appear good to first order and will be refined with spatially denser data sets. Using the residual velocity field as a proxy for permanent deformation, with some caveats, we compare to geologically constrained estimates of Neogene deformation. This yields a remarkably similar spatial pattern of deformation to those suggested on geologic grounds [*Pezzopane and Weldon*, 1993; *Wells et al.*, 1998] and provides direct constraints on current deformation rates.

The convergent margin has three coastal kinematic domains from north to south: a relatively stable Canadian forearc where observed deformation is largely due to subduction zone coupling, the northward-migrating central Cascadia forearc, and Pacific plate entrainment coupled with clockwise rotation or northwestward translation of the southern Cascadia forearc. Strain gradients across Puget Sound–Straits of Juan de Fuca and the Klamath Mountains concentrate crustal deformation that separates the three regions: GPS kinematics indicate 6-7 mm/yr north-south contraction within the Washington forearc, similar in magnitude to shortening across the Los Angeles Basin. Dextral northwest-directed deformation related to penetration of the Eastern California shear zone and Walker Lane transects northern California near the Klamath Mountains and immediately to the south, a result that had not been predicted on geologic grounds.

These kinematic domains correspond to recognized geomorphic provinces within the arc. Increasing evidence from this and related studies indicates no evidence for corresponding seismic segmentation of the subduction zone. Nonetheless, the dynamics of subduction and its obliquity apparently control the distribution of fore-arc deformation domains.

Behind the magmatic front, GPS kinematics reflect the transition from Basin and Range extension and penetration of the Eastern California shear zone to contraction in the Yakima fold belt and a tectonically neutral Canadian back arc.

In the Pacific Northwest, geologic studies are sparse and necessarily overlook structures with no surface expression or poor exposure. Typical lengths of earthquake recurrence intervals are an order of magnitude or more longer than the decades-long history of seismic monitoring. Our study demonstrates the effectiveness of geodesy for rapid determination of the pattern and magnitude of regional deformation and geodetic moment potential.

Acknowledgments. This study was supported by the National Science Foundation (Academic Research Infrastructure, Geophysics and Instrumentation and Facilities Programs) and by the Geological Survey of Canada. Additional GPS observations were provided by the Cascade Volcano Observatory, USGS, the NGS CORS network, and BARD (the Bay Area Regional Deformation Array). Thanks to Mark Murray for allowing us to include data from YBHB. Harvey Kelsey and Pat McCrory were instrumental in siting continuous GPS installations. Earthquake epicenters were taken from the CNSS (Council of the National Seismic System) Worldwide Earthquake Catalog, distributed by the Northern California Earthquake Data Center (NCEDC). Member networks of the Council of the National Seismic System (CNSS) are gratefully acknowledged. This paper has benefited from discussion with Brad Hager, Mark Hemphill-Haley, Gene Humphreys, Harvey Kelsey, Pat McCrory, Tim Melbourne, Andrew Miner, Ray Weldon, and Ray Wells. Reviews by Rick Bennett and John Oldow greatly improved the manuscript. Todd Williams developed the shaded relief map using GMT [*Wessel and Smith*, 1995]. Andrew Miner digitized and compiled the fault map.

References

Adams, J., Paleoseismicity of the Cascadia subduction zone Evidence from turbidites off the Oregon-Washington margin, *Tectonics*, *9*, 569-583, 1990.

Atwater, B. F., Evidence for great Holocene earthquakes along the outer coast of Washington state, *Science*, *236*, 942-944, 1987

Atwater, B. F., and E. Hemphill-Haley, Recurrence intervals for great earthquakes of the past 3,500 years at northeastern Willapa Bay, *U S Geol. Surv. Prof. Pap.*, 108, 1997.

Atwater, B. F., et al , Summary of coastal geologic evidence for past great earthquakes at the Cascadia subduction zone, *Earthquake Spectra*, *II* (1), 1-18, 1995.

Atwater, B F , and D. Yamaguchi, Sudden, probably coseismic submergence of Holocene trees and grass in coastal Washington state, *Geology*, *19*, 706-709, 1991

Bacon, C. R., M. A. Lanphere, and D. E. Champion, Late Quaternary slip rate and seismic hazards of the West Klamath Lake fault zone near Crater Lake, Oregon Cascades, *Geology*, *27*, 43-46, 1999.

Beeson, M. H., and T. L. Tolan, The Columbia River Basalt Group in the Cascade Range: A middle Miocene reference datum for structural analysis, *J Geophys Res.*, *95*, 19,547-19,559, 1990

Bock, Y., S. et al , Southern California permanent GPS geodetic array Continuous measurements of regional crustal deformation between the 1992 Landers earthquake and 1994 Northridge earthquake, *J. Geophys. Res.*, *102*, 18,013-18,033, 1997

Boucher, C., Z. Altamimi, and P. Sillard, The 1997 International Terrestrial Reference Frame (ITRF97), in *IERS Technical Note 27*, Observatoire de Paris, Paris, France, 1999.

Braunmiller, J , J Nabelek, B. Leitner, and A. Qamar, The 1993 Klamath-Falls, Oregon, earthquake sequence: Source mechanisms, *Geophys. Res. Lett.*, *22*, 105-108, 1995.

Bucknam, R. C., E. Hemphill-Haley, and E. B. Leopold, Abrupt uplift within the past 1700 years at southern Puget Sound, Washington, *Science*, *258*, 1611-1614, 1992.

Campbell, N. P., Recurrent Holocene to recent movement in the Toppenish Ridge fault system, south central Washington, *Geol. Soc. Am. Abstr. Programs*, *26* (7), A-187, 1994

Campbell, N P., and R. D Bentley, Late Quaternary deformation of the Toppenish Ridge uplift in south-central Washington, *Geology*, *9*, 519-524, 1981.

Colman, S. M., J. G. Rosenbaum, R L Reynolds,

and S. M. Sarna-Wojcicki, Post-Mazama (7 Ka) faulting beneath Upper Klamath Lake, Oregon, *Bull. Geol. Soc Am*, *90*, 243-247, 2000.

Crosson, R S., Small earthquakes, structure, and tectonics of the Puget Sound region, *Bull. Seismol. Soc. Am*, *62*, 1133-1171, 1972.

Darienzo, M. E., and C. D. Peterson, Magnitude and frequency of subduction-zone earthquakes along the northern Oregon coast in the past 3,000 years, *Oregon Geology*, *57*, 3-12, 1995

DeMets, C, and T. H Dixon, Kinematic models for Pacific-North America motion from 3 Ma to present, I Evidence for steady motion and biases in the NUVEL-1A model, *Geophys. Res Lett*, *26*, 1921-1924, 1999

DeMets, C, R G. Gordon, D F Argus, and S. Stein, Effect of recent revisions to the geomagnetic reversal time-scale on estimates of current plate motions, *Geophys Res. Lett.*, *21*, 2191-2194, 1994.

dePolo, C. M., D. G. Clark, D. B. Slemmons, and A. R. Ramelli, Historical surface faulting in the Basin and Range Province, western North America: Implications for fault segmentation, *J. Struct. Geol.*, *13*, 123-136, 1991

Dixon, T. H., M. M. Miller, F. Farina, H. Wang, and D. J. Johnson, Present-day motion of the Sierra Nevada block, and some implications for Basin and Range tectonics, *Tectonics*, *18*, 1-24, 2000.

Doser, D. I, Source parameters of earthquakes in the Nevada Seismic Zone, 1915-1943, *J. Geophys. Res.*, *93*, 15,001-15,015, 1988

Dragert, H., and R. D. Hyndman, Continuous GPS monitoring of elastic strain in the Northern Cascadia subduction zone, *Geophys. Res. Lett.*, *22*, 755-758, 1995.

Dragert, H., R. D. Hyndman, G. C. Rogers, and K Wang, Current deformation and the width of the seismogenic zone of the northern Cascadia subduction thrust, *J. Geophys Res*, *99*, 653-668, 1994.

Dreger, D., J. Ritsema, and M. Pasyanos, Broadband analysis of the 21 September, 1993 Klamath-Falls earthquake, *Geophys. Res. Lett.*, *22*, 997-1000, 1995.

England, P., and R. E. Wells, Neogene rotations and quasi-continuous deformation of the Pacific Northwest continental margin, *Geology*, *19*, 978-981, 1991.

Fluck, P., R. D. Hyndman, and K. Wang, Three-dimensional dislocation model for great earthquakes of the Cascadia subduction zone, *J. Geophys. Res.*, *102*, 20,539-20,550, 1997.

Freymueller, J. T., M. H. Murray, P. Segall, and D. Castillo, Kinematics of the Pacific-North America plate boundary zone, northern California, *J Geophys. Res.*, *104*, 7419-7441, 1999

Gower, H. D, J. C. Yount, and R S. Crosson, Seismotectonic map of the Puget Sound Region, Washington, *U.S. Geol. Surv Misc. Inv. Map I-1613*, 1985.

Heaton, T. H., and H Kanamori, Seismic potential associated with subduction earthquakes in the northwestern United States, *Bull. Seismol. Soc. Am.*, *74*, 933-941, 1984

Henton, J A., H Dragert, R. D. Hyndman, and K Wang, Geodetic monitoring of crustal deformation on Vancouver Island, *Eos Trans. AGU*, *79*, (45), Fall Meet. Suppl., F192, 1998

Hooper, P. R., and R M. Conrey, A model for the tectonic setting of the Columbia River Basalt eruptions, in *Volcanism and Tectonism in the Columbia River Flood-Basalt Province*, *Spec Pap. Geol. Soc Am*, *239*, 293-306, 1989

Hutter, I. L., The Wallula fault zone and constraints on the timing and nature of deformation along the Olympic-Wallowa lineament, *Geol. Soc Am. Abstr Programs*, *26* (7), A-187, 1994.

Johnson, H. O., and D C. Agnew, Monument motion and measurement of crustal velocities, *Geophys. Res. Lett*, *22*, 2905-2908, 1995

Johnson, S Y, S. V Dadisman, J. R Childs, and W D. Stanley, Active tectonics of the Seattle Fault and central Puget Sound, Washington: Implications for earthquake hazards, *Geol Soc Am. Bull.*, *111*, 1042-1053, 1999

Johnson, S. Y., C. J. Potter, and J. M Armentrout, Origin and evolution of the Seattle basin and Seattle fault, *Geology*, *22*, 71-74, 1994.

Johnson, S. Y., C. J Potter, J M. Armentrout, J J. Miller, C. Finn, and C. S Weaver, The southern Whidbey Island fault An active structure in the Puget Lowland, Washington, *Geol. Soc. Am Bull*, *108* (3), 334-354, 1996.

Kelsey, H. M, and G A. Carver, Late Neogene and Quaternary tectonics associated with northward growth of the San Andreas transform fault, northern California, *J Geophys. Res.*, *93*, 4797-4819, 1988.

Kelsey, H. M., R. L. Ticknor, J. G. Bockheim, and C. E. Mitchell, Quaternary upper plate deformation in coastal Oregon, *Geol. Soc Am. Bull.*, *108*, 843-860, 1996.

Khazaradze, G., A. Qamar, and H Dragert, Tectonic deformation in western Washington from continuous GPS measurements, *Geophys. Res. Lett*, *26*, 3153-3158, 1999.

Langbein, J., and H. Johnson, Correlated errors in geodetic time series: Implications for time-dependent deformation, *J. Geophys. Res.*, *102*, 591-603, 1997.

Ludwin, R. S., C S Weaver, and R. S. Crosson, Seismicity of Washington and Oregon, in *Neotectonics of North America*, edited by D. B. Slemmons, et al., pp. 77-98, Geol. Soc. Am., Boulder, Colo., 1991

Ma, L., R. Crosson, and R. Ludwin, Focal mechanisms of western Washington earthquakes and their relationship to regional tectonic stress, pp. 28, U.S. Geol. Surv, 1991

Ma, L., R. S. Crosson, and R. Ludwin, Western Washington earthquake focal mechanisms and their relationship to regional tectonic stress, in *Assessing earthquake hazards and reducing risk in the Pacific Northwest: Volume 1*, edited by A. M. Rogers, T J. Walsh, W J Kockelman, and G. R. Priest, pp. 257-283, 1996.

Malone, S. D., and S. Bor, Attenuation patterns in the Pacific Northwest based on intensity data and the location of the 1872 North Cascades earthquake, *Bull. Seismol. Soc. Am.*, *69*, 531-546, 1979.

Malone, S. D., E. T Endo, C. S. Weaver, and J. W. Ramey, Seismic monitoring for eruption prediction, *U S. Geol. Surv Prof Pap.*, *1250*, 803-813, 1981.

Malone, S. D., G. H. Rothe, and S. W. Smith, Details of microearthquake swarms in the Columbia Basin, Washington, *Bull. Seismol. Soc. Am.*, *65*, 855-864, 1975

Mann, G. M., and C. E. Meyer, Late Cenozoic structure and correlations to seismicity along the Olympic-Wallowa lineament, *Geol Soc. Am Bull.*, *105*, 853-871, 1993.

Mao, A., C. G A. Harrison, and T. Dixon, Noise in GPS coordinate time series, *J. Geophys. Res.*, *104*, 2797-2816, 1999.

McCaffrey, R, M. D. Long, C Goldfinger, P. C. Zwick, J. L. Nabelek, C. K Johnson, and C. Smith, Rotation and plate locking at the southern Cascadia subduction zone, *Geophys Res Lett.*, *27*, 3117-3120, 2000.

McCrory, P. A, Tectonic model explaining divergent contraction directions along the Cascadia subduction margin, Washington, *Geology*, *24*, 929-932, 1996.

McCrory, P. A, Upper plate contraction north of the migrating Mendocino triple junction, northern California: Implications for partitioning of strain, *Tectonics*, *19*, 1144-1160, 2000.

Miller, M. M, et al., Precise measurements help gauge Pacific Northwest's earthquake potential, *Eos Trans AGU*, *79*, 269, 275, 1998.

Miller, M. M., D J Johnson, T. H. Dixon, and R K Dokka, Refined kinematics of the Eastern California shear zone from GPS observations, 1993-1998, *J. Geophys Res*, *105*, 2245-2264, 2001

Milne, W. G, Seismic activity in Canada west of the 113th meridian, 1841-1951, pp. 126-127, Dominion Obs., Ottawa, Ontario, Canada,1956.

Murray, M H., and M. Lisowski, Strain accumulation along the Cascadia subduction zone, *Geophys. Res Lett.*, *27*, 3631-3634, 2000.

Nabelek, J, and G Y Xia, Moment-tensor analysis using regional data-Application to the 25-March-1993, Scotts-Mills, Oregon, earthquake, *Geophys. Res Lett.*, *22*, 13-16, 1995

Nelson, C H, C. Goldfinger, J E Johnson, and G Dunhill, Variation of modern turbidite systems along the subduction zone margin of Cascadia Basin and implications for turbidite reservoir beds, in *Deep-water Reservoirs of the World*, edited by P. W. Weimer, and C H. Nelson, pp 31, Houston, Tex., 2000

Noson, L. L, A Qamar, and G W Thorsen, Washington State earthquake hazards, *Wash Div Geol. Earth Resour, Inf Circ.*, *85*, 77, 1988

Oldow, J S., C. L V. Aiken, J. L. Hare, J. F Ferguson, and R F. Hardyman, Active displacement transfer and differential block motion within the central Walker Lane, western Great Basin, *Geology*, *29*, 19-22, 2001

Patton, H. J., *P*-wave fault-plane solutions and the generation of surface waves by earthquakes in the western United States, *Geophys Res. Lett*, *12*, 518-521, 1985

Pezzopane, S. K., and R Weldon, Tectonic role of active faulting in central Oregon, *Tectonics*, *12*, 1140-1169, 1993.

Pratt, T. L., S. Y. Johnson, C J. Potter, W. J. Stephenson, and C A Finn, Seismic reflection images beneath Puget Sound, western Washington State The Puget Lowland thrust sheet hypothesis, *J Geophys. Res*, *102*, 27,469-27,489, 1997

Qamar, A., R Ludwin, R S Crosson, and S. D. Malone, Earthquake hypocenters in Washington and northern Oregon, 1982-1986, Dept. Nat. Resour., Wash Div of Geol. and Earth Resour., Olympia, Wash, 1987.

Raisz, E, The Olympic-Wallowa lineament, *Am. J. Sci.*, *243-A*, 479-485, 1945

Reidel, S., The Saddle Mountains: The evolution of an anticline in the Yakima fold belt, *Am J. Sci.*, *284*, 942-977, 1984

Riddihough, C R, Recent movements of the Juan de Fuca plate system, *J Geophys. Res*, *89*, 6980-6994, 1984

Satake, K., K. Shimizaki, Y Tsuji, and K Ueda, Time and size of a giant earthquake in Cascadia inferred from Japanese tsunami records of January 1700, *Nature*, *379*, 246-249, 1996.

Savage, J C., A dislocation model of strain accumulation and release at a subduction zone, *J. Geophys Res*, *88*, 4984-4996, 1983.

Savage, J C., J L. Svarc, W. H Prescott, and M. H Murray, Deformation across the forearc of the Cascadia subduction zone at Cape Blanco, Oregon, *J Geophys Res*, *105*, 3095-3102, 2000

Slemmons, D B., E R Engdahl, M D Zoback, and D. D Blackwell, Neotectonics of North America, in *Decade of North American Geology*, pp 498, Geol. Soc Am, Boulder, Colo, 1991

Smith, W. H F, and D T Sandwell, Global seafloor topography from satellite altimetry and ship depth soundings, *Science*, *277*, 1957-1962, 1997.

Stanley, W D, S Y. Johnson, A I Qamar, C. S. Weaver, and J M Williams, Tectonics and seismicity of the southern Washington Cascade Range, *Bull Seismol Soc Am*, *86*, 1-18, 1996

Tolan, T L., and S. P Reidel, Structure map of a portion of the Columbia River flood basalt province, in Volcanism and Tectonism in the Columbia River Flood Basalt Province, *Spec. Pap. Geol Soc Am , 239*, 386, 1989

Wallace, R E , Patterns and timing of Late Quaternary faulting in the Great Basin Province and relation to some regional tectonic features, *J. Geophys Res., 89*, 5763-5769, 1984.

Wang, K., Simplified analysis of horizontal stresses in a buttressed forearc sliver at an oblique subduction zone, *Geophys Res Lett., 23*, 2021-2024, 1996.

Wang, K , J He, H Dragert, and T James, Three-dimensional viscoelastic interseismic deformation model for the Cascadia subduction zone, *Earth Planet Space, in press*, 2000

Wang, K., T Mulder, G C. Rogers, and R D Hyndman, Case for very low coupling stress on the Cascadia subduction fault, *J Geophys Res., 100*, 12,907-12,918, 1995.

Wdowinski, S , Y Bock, J Zhang, P. Fang, and J Genrich, Southern California Permanent GPS Geodetic Array: Spatial filtering of daily positions for estimating coseismic and postseismic displacements induced by the Landers earthquake, *J. Geophys Res , 102*, 18,057-18,070, 1997.

Weaver, C S., W C. Grant, S D. Malone, and E. T Endo, Post May 18, 1980, seismicity. Volcanic and tectonic implications, in *The 1980 eruptions of Mount St Helens, Washington, U S Geol Surv. Prof Pap , 1250*, 109-121, 1981.

Weaver, C. S , and S W Smith, Regional tectonic and earthquake hazard implications of a crustal fault zone in southwestern Washington, *J. Geophys Res , 88*, 10,371-10,383, 1983

Wells, R. E , Paleomagnetic rotations and the Cenozoic tectonics of the Cascade Arc, Washington, Oregon, and California, *J Geophys Res , 95*, 19,409-19,417, 1990

Wells, R E , C. S Weaver, and R. J Blakely, Forearc migration in Cascadia and its neotectonic significance, *Geology, 26*, 759-762, 1998.

Wessel, P , and W H. F Smith, New version of the Generic Mapping Tools released, *Eos Trans AGU, 76*, (33), 329. 1995

West, M W , F X. Ashland, A J Bussacca, G. W Berger, and M E. Shaffer, Late Quaternary deformation, Saddle Mountains anticline, south-central Washington, *Geology, 24*, 1123-1126, 1996

Wilson, D S , Deformation of the so-called Gorda plate, *J Geophys Res., 94*, 3065-3075, 1989

Wilson, D. S , Confidence-intervals for motion and deformation of the Juan-de-Fuca plate, *J Geophys. Res , 98*, 16,053-16,071, 1993

Yamaguchi, D. K , B F. Atwater, D E Bunker, B E Benson, and M S Reid, Tree-ring dating the 1700 Cascadia earthquake, *Nature, 389*, 922-923, 1997.

Zollweg, J E., and R S Jacobson, A seismic zone on the Oregon-Idaho border The Powder River earthquakes of 1984, *Bull Seismol Soc Am., 76*, 985-999, 1986.

Zumberge, J , M. B. Heflin, D C Jefferson, M M Watkins, and F H. Webb, Precise point positioning for the efficient and robust analysis of GPS data from large networks, *J Geophys Res , 102*, 5005-5017, 1997

H Dragert and K L Wang, Geological Survey of Canada, Pacific Geoscience Centre, 9860 W Saanich Road, Sidney, British Columbia, Canada V8L 4B2

D J. Johnson, M M. Miller, and C M Rubin, Department of Geological Sciences, Central Washington University, 400 E. Eighth Avenue, Ellensburg, WA 98926 (meghan@cwu edu)

A Qamar, Geophysics Program, University of Washington, Box 351650, Seattle, WA 98195

C Goldfinger, College of Oceanic and Atmospheric Sciences, Oregon State University, 104 Ocean Administration Building, Corvallis, OR 97331

(Received April 5, 2000;
revised December 8, 2000,
accepted December 11, 2000.)